

Influence of steps on the tilting and adsorption dynamics of ordered pentacene films on vicinal Ag(111) surfaces

E. Mete,^{1,*} İ. Demiroğlu,² E. Albayrak,³ G. Bracco,⁴ Ş. Ellialtıoğlu,⁵ and M. F. Danişman^{2,†}

¹*Department of Physics, Balıkesir University, Balıkesir 10145, Turkey*

²*Department of Chemistry, Middle East Technical University, Ankara 06800, Turkey*

³*Department of Physics, Sakarya University, Sakarya, Turkey*

⁴*CNR-IMEM and Department of Physics, University of Genoa, via Dodecaneso 33, 16146 Genoa, Italy*

⁵*Department of Physics, Middle East Technical University, Ankara 06800, Turkey*

(Dated: August 28, 2018)

Here we present a structural study of pentacene (Pn) thin films on vicinal Ag(111) surfaces by He atom diffraction measurements and density functional theory (DFT) calculations supplemented with van der Waals (vdW) interactions. Our He atom diffraction results suggest initial adsorption at the step edges evidenced by initial slow specular reflection intensity decay rate as a function of Pn deposition time. In parallel with the experimental findings, our DFT+vdW calculations predict the step edges as the most stable adsorption site on the surface. An isolated molecule adsorbs as tilted on the step edge with a binding energy of 1.4 eV. In addition, a complete monolayer (ML) with pentacenes flat on the terraces and tilted only at the step edges is found to be more stable than one with all lying flat or tilted molecules, which in turn influences multilayers. Hence our results suggest that step edges can trap Pn molecules and act as nucleation sites for the growth of ordered thin films with a crystal structure similar to that of bulk Pn.

PACS numbers: 82.45.Mp, 68.55.-a, 73.21.Ac, 71.15.Mb, 68.47.Fg

Pentacene thin films are still being studied heavily due to their potential electronic device applications and being a model system for organic semiconductor film studies.[1–3] On many different metal surfaces, Pn is reported to form lying down films with similar unit cell structures.[4–14] In case of the second or higher layers however, even on the same metal surface, different growth mechanisms and/or dynamics have been reported.[4, 8, 9, 15–17] On Ag(111), while some reports suggest a bilayer film formation, where an ordered second layer with the symmetry of the Ag(111) surface forms on top of a disordered (2D gas phase) first layer at room temperature, some others suggest formation of bulk like Pn structures immediately after the first ML).[4, 16, 17] In addition, in our earlier works we had shown that an ordered Pn multilayer could only be formed on a relatively high step density Ag(111) surface and the multilayer order can be improved by increasing the kinetic energy (KE) of the molecules, by seeded supersonic molecular beam (SSMB) deposition.[13] This observation was attributed to step edges acting as nucleation centers for tilted molecules in the multilayers resulting in a step flow growth mechanism. Such growth dynamics was also observed for different planar organic molecules on vicinal copper and gold surfaces by different groups.[18–20] In addition, high energy of the molecules was suggested to result in a local annealing effect which in turn helps formation of ordered multilayers at low substrate temperatures. These experimental results were in line with our recent theoretical work on Pn on flat Ag(111) surface where a multilayer structure with tilted Pn molecules was found to be more stable than one with flat lying molecules.[21] However during the above mentioned experimental studies surface

step density was changed arbitrarily by using a miscut Ag(111) surface and the molecular KEs were not measured by a time of flight (TOF) method but only estimated by using a theoretical formula.[13] The necessity to test the stable configuration and the contradictions in the literature have stimulated the present experimental work on Pn film growth on Ag(11,12,12) surface complemented by density functional theory (DFT) calculations to explore the effect of surface step density and molecular energy on the Pn film growth with the aim to improve our understanding of such systems.

Pn films were grown by using SSMB deposition and characterized with a low energy atom diffraction (LEAD) apparatus both of which were detailed before.[12, 22] KE of the molecules was controlled by changing the nozzle temperature of the SSMB source and the carrier gas (CG). A commercial quartz crystal microbalance (QCM) and a quadruple mass spectrometer were implemented on this apparatus for allowing molecular flux and TOF measurements. In addition, a gold covered electrode of a custom design QCM can be used as the active substrate to simultaneously measure He specular intensity decay and record resonance frequency shift of the substrate to estimate film coverage during deposition.[23] Pentacene KEs, determined by TOF measurements, for standard SSMB source conditions were 2.2 eV for He CG and 0.2 eV for Kr CG. For LEAD measurements a monoenergetic He beam, with energy of 14 meV (incident wave vector $k_i=5.13 \text{ \AA}^{-1}$) and velocity dispersion of 2%, was scattered for the sample surface and the angular distribution of the scattering intensity was recorded. For reciprocal space mapping the diffraction spectra, recorded at 80 K surface temperature along different crystallographic di-

rections, were converted to momentum by using the equation $\Delta K_{\parallel} = k_i(\sin \theta_f - \sin \theta_i)$ where ΔK_{\parallel} is the parallel momentum transfer, and θ_i and θ_f are the incident angle and the detector angular position, respectively. The reference “flat” Ag(111) and the Ag(11,12,12) substrates were purchased from Mateck GmbH with an orientation accuracy of $<0.1^\circ$ and had specular reflection intensity values of 60 % and 45 % of the incident beam respectively. Ag(11,12,12) has a miscut of 2.31° with respect to Ag(111) surface normal, with (111) terraces of 24 rows (58 Å) wide with step edges parallel to $[01\bar{1}]$ direction and perpendicular to $[\bar{2}11]$ direction.

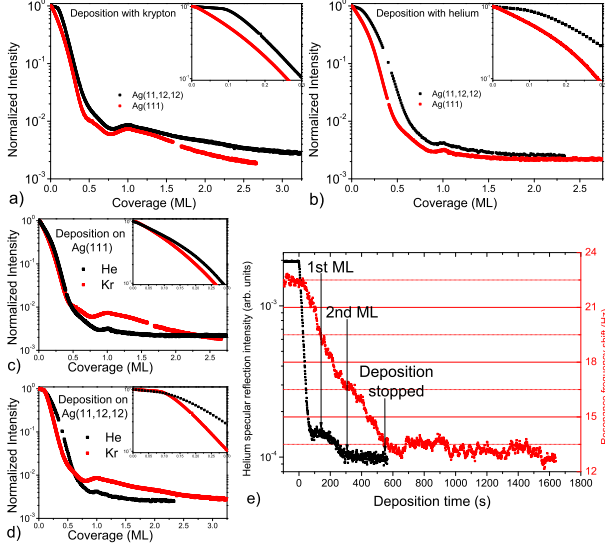


FIG. 1. Specular reflection intensity decay curves as function of Pn coverage. (a-d) Insets show the initial decay region. ($k_i=5.13 \text{ \AA}^{-1}$, incidence angle is 56° for Ag(111) and 59° for Ag(11,12,12), deposition temperature 200 K, on Ag(11,12,12) molecular beam direction was parallel to step edges) In (e) specular reflection intensity decay curve and resonance frequency shift from the gold electrode surface of a quartz crystal during Pn film deposition is shown.

In Fig.1 we show He specular reflection intensity decay curves as a function of film coverage, at 200 K substrate temperature, for different surfaces and deposition energies. The coverage values were deduced from the specular reflection recovery peaks, with the assumption that these peaks correspond to ML completion. In fact, a similar recovery peak was measured on Au(111) electrode surface of a quartz crystal at a resonance frequency shift (2.9 Hz) corresponding to a deposited ML of Pn as shown in Fig.1e. When the initial part of these curves are examined it can be seen that, regardless of the type of the CG, on Ag(11,12,12) there is a slow decay up to about 0.12 ML that is due to initial Pn adsorption to step edges. In fact, the He reflectivity is very sensitive to molecular adsorbed species[24] and this slow decay can be attributed to the overlapping of Pn cross sections (σ) with that of silver step edges resulting in a decrease of the

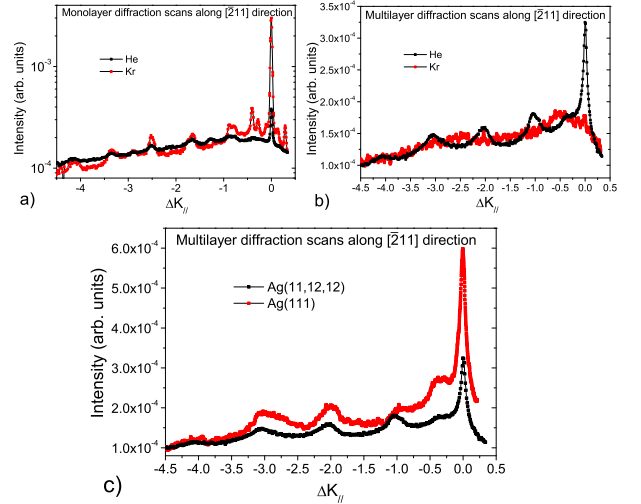


FIG. 2. Helium diffraction scans of mono (a) and multilayers (b) of Pn on Ag(11,12,12) with different KEs. Comparison of multilayer diffraction scans on Ag(11,12,12) and Ag(111) grown with high KE are shown in (c). ($k_i=5.13 \text{ \AA}^{-1}$, incidence angle is 56° for Ag(111) and 59° for Ag(11,12,12))

effective cross section (σ_{eff}) of Pn molecules. However on Ag(111) due to lack of steps, Pn molecules mainly adsorb on the terraces and present a larger σ_{eff} to incoming He atoms which results in a faster decay of specular intensity. On the 24 rows wide terraces of Ag(11,12,12), 8 Pn rows with a 6×3 unit cell are expected to adsorb at full coverage[13, 21] and a single Pn row is necessary to saturate the steps, corresponding to a coverage $1/8$ (0.125) ML. For higher coverage, Pn starts to fill terraces and the decay is faster explaining the observed specular intensity trend. In addition, when deposition is performed at 80 K substrate temperature, the slow decay region is completely missing due to reduced diffusion length of Pn molecules which prevent them to reach to the step edges. Regardless of the surface step density, the reflectivity decay curves for coverages of >0.3 ML show that deposition with Kr yields a smoother ML as indicated by the higher specular reflection intensity level. This can be due to disordering of the Ag step edges and terraces caused by the high energy of the Pn molecules deposited with He CG. In fact for Ag(111) surface, energies needed to detach an atom from a step edge (0.49-0.76 eV) or to diffuse an atom along the step (0.29-0.34 eV)[25, 26] are all much lower than Pn KEs deposited with He. Whereas in case of Kr CG, Pn molecules do not have enough energy to activate these roughening processes. In fact Pn σ_{eff} s on Ag(11,12,12) (Fig 1d), calculated by maximal attraction model proposed by Comsa[24], increases from $\sigma_{\text{Kr}} = 102 \pm 3 \text{ \AA}^2$ to $\sigma_{\text{He}} = 156 \pm 4 \text{ \AA}^2$ for deposition with Kr and He respectively. When deposition was performed with a He beam perpendicular to step edges, σ_{He} further increases to $328 \pm 2 \text{ \AA}^2$, which indicates that step edge roughening is more effective in case of perpendicu-

lar deposition. These values can be compared with the Pn vdW cross section, $\sigma_{\text{vdW}}=124 \text{ \AA}^2$ [27]– 119 \AA^2 [28]. After the completion of the first ML, specularity decreases much faster in the case of Kr CG on both surfaces. This suggests that though the ML is more ordered/smooth with Kr, an ordered second layer does not grow on it.

Diffraction scans, obtained from the MLs and the multilayers grown with different KEs and on different substrates, shown in Fig. 2 confirm the above mentioned mechanism: On Ag(11,12,12) while the ML diffraction peaks and specularity are more intense with Kr CG, no multilayer diffraction peaks could be observed. A peak width analysis indicates that average ML domain size with He beam is about 50 \AA whereas with Kr it is about 70 \AA which means that with both CGs the domains extend as wide as the terrace width of the Ag(11,12,12) surface. With He, however, multilayer diffraction peaks which are consistent with previously reported[12, 13] Pn multilayer structure could be observed. Finally when the multilayer structure on Ag(111) and Ag(11,12,12) are compared it can be seen that, though less intense, the diffraction peaks are slightly narrower on Ag(11,12,12), corresponding to domain size of 17 \AA on Ag(111) and 24 \AA on Ag(11,12,12). The reason for low specular reflection and diffraction peak intensities on the vicinal surface may be the higher level of diffuse scattering due to step edges, as discussed above.

To gain further insights on the system, we performed DFT calculations. Pure DFT methods underestimate the adsorption energy of Pn molecules on Ag(111). Among these, GGA-PW92 functional[29] gives still low but slightly better binding energies and bond lengths for isolated and ML cases on Ag(111) surface.[21] DFT calculations were performed using VASP[30] with projector augmented waves (PAW) method[31, 32]. We employed Grimme’s semiempirical forcefield approach[33] to include long range vdW corrections to better describe the interaction of Pn molecules with Ag substrate. We used

TABLE I. DFT+vdW results of Pn on vicinal Ag(111) surface for different coverage models. E_t is the relative supercell total energy. Pn–step edge bond length is denoted by l . Labels denote the layer numbers for interlayer separations, d_1 , d_{1-2} and for tilting angles α_1 , α_2 , respectively.

	Model	E_t (eV)	l (\AA)	d_1 (\AA)	d_{1-2} (\AA)	α_1 ($^\circ$)	α_2 ($^\circ$)
Single	flat@bridge	0.00	–	2.92	–	0.0	–
	C@step	-0.47	2.55	–	–	25.4	–
1ML	flat	0.00	2.63	2.94	–	0.0	–
	flat2 ^a	-0.51	2.49	2.94	–	0.0	–
2ML	flat-tilt	0.00	2.54	2.77	2.56	0.0	17.0
	flat2 ^a -tilt	-0.49	2.50	2.77	2.56	0.0	-13.1

^a molecules flat on the terrace, tilted at the step edge.

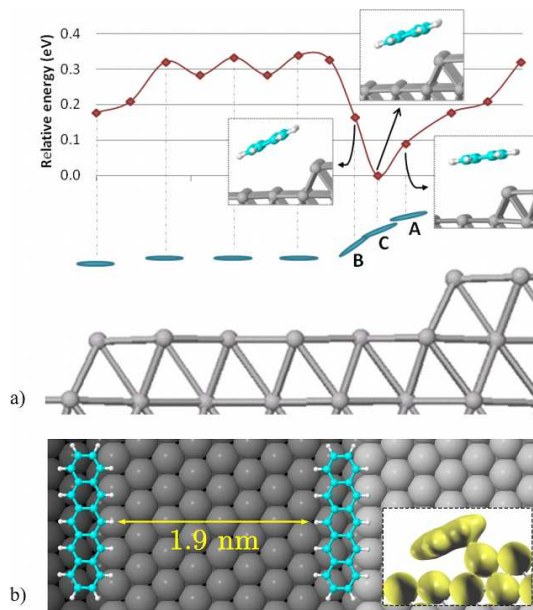


FIG. 3. (a) Potential energy profile of single Pn on Ag(233) vicinal surface along $[211]$ direction (A,B,C configurations shown in the corresponding insets), (b) the minimum energy configuration of an isolated Pn at the step edge on Ag(455) surface (the charge density is presented in the inset).

a 4 layer slab to model the vicinal Ag(111) surface with two different terrace sizes. The width of the terraces on Ag(233) and Ag(455) supercells measure 10.0 \AA and 20.0 \AA spanning six and ten surface Ag atoms along $[211]$, respectively. Ag(233) supercell has been used to study the potential energy profile of an isolated Pn as schematically shown in Fig.3a. Ag(455) slab for one and two ML coverages allows to place three Pn molecules one being at the step edge as depicted in Fig.4. We have relaxed all probable configurations based on minimization of the forces requiring them to be smaller than 0.1 eV \AA^{-1} on every atom. In order to elucidate the effect of van der Waals contribution on Pn-metal interaction that characterizes the minimum energy structures, we carried out these calculations both with and without dispersive energy corrections.

Pn molecules give noticeably stronger binding at the step edges relative to that on the flat terraces as seen in Fig.3a which shows the diffusion barrier profile along $[211]$ obtained with DFT. Pn at the step edge bends along its long axis such that the middle part of the molecule gets slightly more closer to the surface from where we measure Pn–step edge bond length (column l in Table I). The curvature is similar to the one observed for Pn on Cu(111) surface. [34] DFT+vdW reproduces this curvature that indicates a strong adsorption. Binding energies at the step edge (case C in Fig.3a) and at the bridge site (molecular center on a Ag-Ag bond) on the terrace are 1.40 and 0.92 eV , respectively. These were much lower with pure DFT. For instance, DFT predicts the binding

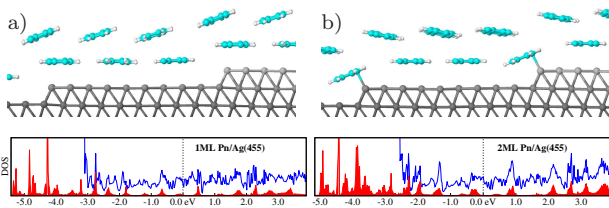


FIG. 4. Relaxed geometries of 2ML Pn on Ag(455) for (a) flat-tilt and (b) flat2-tilt cases. Densities of states (DOS) are presented for the flat2 and flat2-tilt structures where the shaded regions are Pn contributions.

energy at the step edge to be 0.62 eV with no bending.

For the first ML, we have considered tilted, flat and flat2 models as initial structures for geometry optimization. In tilted case all molecules are tilted around their major axes. Flat model is as the first layer of Fig.4a where all Pn molecules lie parallel to the Ag surface plane. Flat2 case differs from the flat one in only that the Pn at the step edge is tilted as in the most stable case C of an isolated molecule (see the first layer of Fig.4b). Pure DFT predicts tilted formation to be the minimum energy configuration while DFT+vdW relaxes tilted case to flat2 one. Moreover, the measured σ_{effs} provide a further support to flat2 model because Pn covers completely a step edge and the tilting reduce the σ to $\sigma_{\text{vdW}} \cos(25.4) = 112$ Å which is at most 10% greater than σ_{Kr} . In the flat model, the σ_{vdW} is increased by the step edge cross section, so, apparently the σ_{He} supports the flat case. But the experimental evidence that He deposition causes an increased disorder and further calculations that exclude the presence of other configurations with minimal energy similar to flat2, leaves flat2 as the only possibility.

Then we considered a second ML which can be tilted or flat as an initial configuration. For 2ML Pn on Ag(455), pure DFT predicts tilted-tilted model to be the lowest energy structure. When the geometry optimization repeated with dispersive corrections, tilted molecules on the terrace become flat leading to flat2-tilt configuration (Fig.4b). Therefore, second ML is tilted while first layer lies flat similar to that of the 1ML case. This is in good agreement with the proposed model for bilayer Pn on Cu(111) from STM/STS measurements.[34] This indicates the role of the step edge in bulk-like formation of Pn molecules beyond the second ML. As a trend, energy differences between flat and flat2 cases for both 1ML and 2ML coverages follow from that of single molecule adsorption cases, *i.e.* flat@terrace and C@step as presented in Table I. Moreover, a comparison of DOS structures for Ag(455) in Fig.4 with those obtained for Ag(111) without steps[21] shows that the difference between the HOMO level of Pn and the Fermi energy of the surface decreases. This suggests an enhanced charge carrier injection at Pn-metal interface in favor of the vicinal surface.

In summary, by using He diffraction and QCM techniques simultaneously and performing DFT+vdW calcu-

lations we have, unambiguously, shown that step edges on Ag(111) surfaces act as nucleation centers for formation of bulk-like Pn thin films on MLs composed of flat lying molecules. This mechanism can be considered to be a rather general one since our results are in line with those reported on different metal surfaces such as Au and Cu. Our results highlight the importance of a) vdW forces for systems with relatively weak interactions like Pn/metal interfaces and b) the effects of metal substrate surface morphology on the crystal and electronic structure of organic semiconductor films which have very important implications on the performance of electronic devices that employ these metal/organic interfaces.

This work was partially supported by TÜBİTAK Grant Nos. 107T408 and 209T084.

* emete@balikesir.edu.tr

† danisman@metu.edu.tr

- [1] J. E. Anthony, *Angew. Chem. Int. Ed.* **47**, 452 (2008).
- [2] A. Facchetti, *Materials Today* **10**, 28 (2007).
- [3] A. Troisi, *Chem. Soc. Rev.* **40**, 2347 (2011).
- [4] D. Kafer, G. Witte, *Chem. Phys. Lett.* **442**, 376 (2007).
- [5] C. Baldacchini *et al.*, *Surf. Sci.* **601**, 2603 (2007).
- [6] C. B. France *et al.*, *Nano Lett.* **2**, 693 (2002).
- [7] P. Guaino *et al.*, *Appl. Phys. Lett.* **85**, 2777 (2004).
- [8] J. H. Kang, X. Y. Zhu, *Appl. Phys. Lett.* **82**, 3248 (2003).
- [9] J. H. Kang, X. Y. Zhu, *Chem. Mater.* **18**, 1318 (2006).
- [10] C. B. France *et al.*, *Langmuir* **19**, 1274 (2003).
- [11] D. Kafer *et al.*, *Phys. Rev. B* **75**, 085309 (2007).
- [12] L. Casalis *et al.*, *Phys. Rev. Lett.* **90**, 26101 (2003).
- [13] M. F. Danisman *et al.*, *Phys. Rev. B* **72**, 085404 (2005).
- [14] M. Pedio *et al.*, *Appl. Surf. Sci.* **254**, 103 (2007).
- [15] G. Beemink *et al.*, *Appl. Phys. Lett.* **85**, 398 (2004).
- [16] M. Eremtchenko *et al.*, *Phys. Rev. B* **72**, 115430 (2005).
- [17] D.B.Dougherty *et al.*, *J.Phys. Chem. C* **112**, 20334 (2008).
- [18] L. Gavioli *et al.*, *Phys. Rev. B* **72**, 035458 (2005).
- [19] M. M. Kamna *et al.*, *Surf. Sci.* **419**, 12 (1998).
- [20] M. E. Canas-Ventura *et al.*, *Angew. Chem. Int. Ed.* **46**, 1814 (2007).
- [21] E. Mete *et al.*, *J. Phys. Chem. C* **114**, 2724 (2010).
- [22] M.F.Danisman *et al.*, *J.Phys. Chem. B* **106**, 11771 (2002).
- [23] M. F. Danisman, B. Ozkan, *Rev. Sci. Instrum.* **82**, 115104 (2011).
- [24] G. Comsa in *Atomic & Molecular Beam Methods*, Vol.2, G. Scoles (Ed.), p.463, Oxford Univ. Press, NY, 1992.
- [25] G. Nandipati, A. Kara, S. I. Shah, T. S. Rahman, *J. Phys. : Condens. Matter*, **23**, 262001 (2011).
- [26] Z. Chvoj, C. Ghosh, T. S. Rahman, M. C. Tringides, *J. Phys. : Condens. Matter* **15**, 5223 (2003).
- [27] A. Bondi, *J. Phys. Chem.* **68**, 44 (1964).
- [28] R. A. Klein, *Chem. Phys. Lett.* **425**, 128 (2006).
- [29] J. P. Perdew, Y. Wang, *Phys. Rev. B* **45**, 13244 (1992).
- [30] G. Kresse and J. Hafner, *Phys. Rev. B*, **47**, 558 (1993).
- [31] P.E. Blöchl, *Phys. Rev. B* **50**, 17953 (1994).
- [32] G. Kresse and J. Joubert, *Phys. Rev. B* **59**, 1758 (1999).
- [33] S. Grimme, *J. Comput. Chem.* **27**, 1787 (2006).
- [34] J. A. Smerdon *et al.*, *Phys. Rev. B* **84**, 165436 (2011).